Supporting Material

The auto-depalmitoylating activity of APT maintains the spatial organization of palmitoylated membrane proteins

Nachiket Vartak[1], Bjoern Papke[1], Hernan E. Grecco[1], Lisaweta Rossmannek[1], Herbert Waldmann[2,3], Christian Hedberg[2], Philippe I.H. Bastiaens[1,3*]

[1]Department of Systemic Cell Biology

Max Planck Institute for Molecular Physiology, Dortmund, Germany

[2]Department of Chemical Biology

Max Planck Institute for Molecular Physiology, Dortmund, Germany

[3]Faculty of Chemistry

Technical University Dortmund, Germany

Contact : Philippe Bastiaens (Corresponding Author)

Email: philippe.bastiaens@mpi-dortmund.mpg.de

SUPPORTING MATERIAL

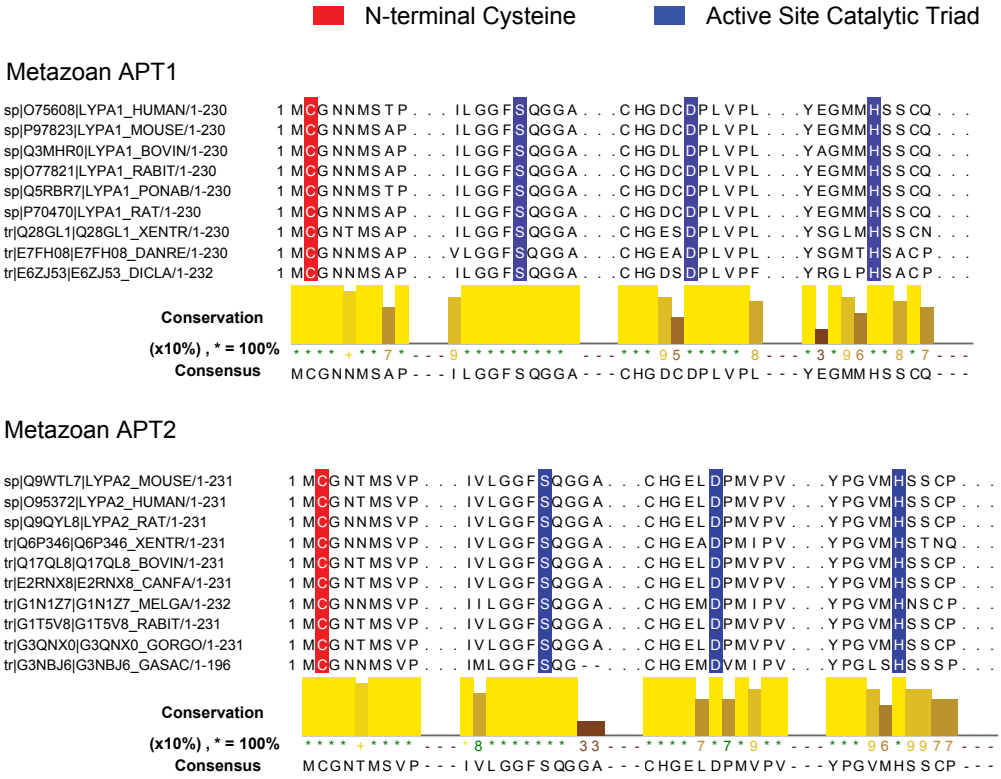

Figure S1: The N-terminal Cysteine of APTs is conserved. Sequence alignments show that the conservation of the Cys-2 residue (red) in metazoan APTs is equivalent to the conservation of the Ser-His-Asp catalytic triad (blue) in the APT active site. The list of sequences presented is the non-redundant (<95% similarity) subset of all available APT1 and APT2 sequences. Sequence nomenclature is in the format "database|accession-id|sequence-id_species-id/full-sequence-length".

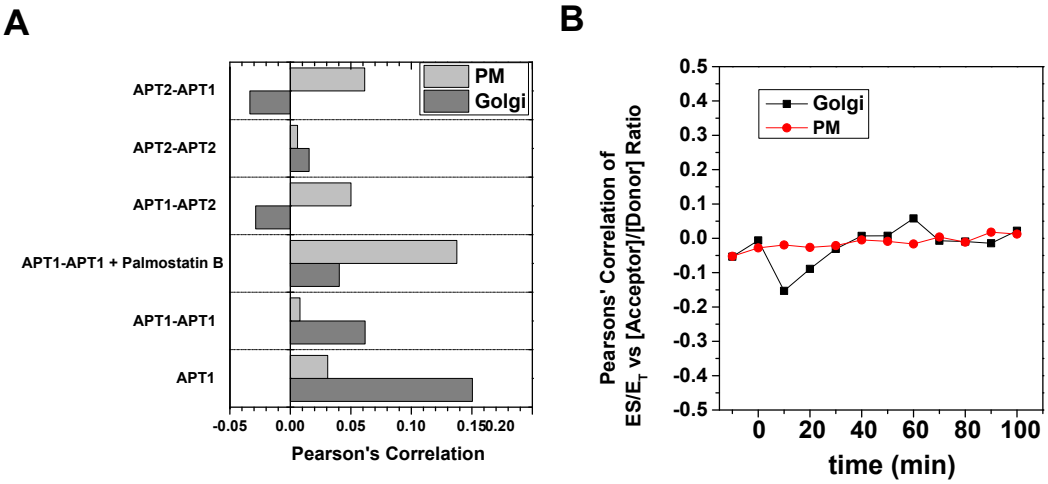

Figure S2: A. Graph shows Pearson's Correlation between ES/ET and Acceptor/Donor ratio on the Golgi and the PM for APT FLIM measurements exemplified in Figure 4. **B.** Graph shows Pearson's Correlation between ES/ET and Acceptor/Donor ratio on the Golgi and the PM over the entire Palmostatin B incubation exemplified in Figure 5*A*.

Supporting Methods

Plasmids and molecular biology

mCitrine fusions of APTs were generated by restriction-ligation of APT1 and APT2 inserts into pcDNA3.1-N1 (Clontech) containing a mCitrine fluorophore. mCherry-fusions to APTs were obtained by replacing the CFP with AgeI/BsrGI fragments of APT1/2-mCFP. mCitrine fusions of APT1S119A, APT1C2S, APT2S122A and APT2C2S were generated by site-directed mutagenesis of APT1- and APT2-mCitrine fusions. Gα(1-11)-mCherry was generated by insertion of an EcoRI/AgeI fragment encoding the first 11 amino acids of $G\alpha_i1$ into mCherry-C1. mCherry-KRas was generated by cloning KRas full length into mCherry-N1. mCherry-C1 or -N1 was generated by inserting an AgeI/BsrGI PCR fragment of mCherry cDNA (gift from R. Tsien) into pEGFP-N1 or pEGFP-C1 (Clontech), respectively. GalT-Cerulean and GalT-mCherry encode a fragment of β-1,4-galactosyltransferase fused to mCerulean or mCherry, respectively. His-tagged APTs were generated by cloning APT genes into pOPIN-N-His vectors (Clontech).

Cell culture, cell transfection and inhibitor treatments

MDCK cells were maintained in MEM supplemented with 10 % foetal bovine serum (FBS). Transfection of plasmids was achieved using Effectene Reagent (Qiagen) according to the manufacturer's protocol. For live cell microscopy, cells were cultured on 35-mm glass bottom dishes (MatTek, Ashland, USA). Palmostatin B (final concentration: 5 μM) and 2-bromopalmitate (final concentration: 50 μM) were prediluted 1:100 and directly added to the imaging medium.

FRAP imaging and quantification

Pre-bleach and post-bleach imaging was typically performed at similar settings, with image acquisition rate optimized by preliminary experiments to minimize monitor bleaching and maximize signal-to-background ratio. Bleaching was performed in a pre-defined region of interest (ROI) on the Golgi apparatus, which was identified by expression of the GalT-mCerulean Golgi marker. For the bleaching step, the laser scanner on the microscope was set to restrict illumination to the ROI with laser intensity sufficient to diminish fluorescence intensity in the ROI to <20% within 1s.
Images were stored as 16-bit TIFF files and background correction was performed by subtracting the peak background intensity of the image histogram plus two standard deviations from the images (1). The images were then median-filtered with a 1-pixel neighbourhood and converted to 32-bit floating point TIFFs without interpolation. Thresholding was then performed to convert background zero-values to Not-a-Number (NaN).

ROI coordinates were retrieved from metadata produced by the microscope acquisition software. After image processing as described above, mean intensities in the ROI of the mCitrine channel yielded recovery of fluorescence after photobleaching as a function of time. The fluorescence intensities were normalized to the fluorescence of the Golgi marker in the

mCerulean channel to account for changes in the organelle structure resulting from the dynamic nature of live cells. The mean fluorescence intensity in the recovery phase in individual cells was fitted as a function of time to the following exponential function [1] that accounts for linear monitor bleaching (2, 3). Half times of fluorescence recovery in the bleached ROI were calculated from the fit-derived values of τ [2]:

$$I_t / I_0 = I_\infty [1-e^{(-x/t)}] - k_b t \qquad [1]$$

$$t_{½} = \tau \ln 2 \qquad [2]$$

Where I_t is the fluorescence intensity (in arbitrary units) at time t (s), I_0 is the residual intensity in the ROI after photobleaching, I_∞ is the fluorescence intensity asymptotically reached at $t = \infty$, τ (s) is the exponential recovery time constant, $t_{1/2}$ (s) is the half time of fluorescence recovery and k_b (s^{-1}) is the monitor bleaching rate constant.

In order to improve precision of the four-parameter fit, global fitting was performed by linking the exponential recovery time parameter across multiple experiments (4). A rigorous error analysis was performed to find the range of the recovery parameter at a confidence interval of 1 standard deviation (5).

FRET-FLIM based enzyme-substrate imaging of APT activity

Briefly, the frequency domain representation of the TCSPC data was obtained by computing the first harmonic of the fluorescence decay in each pixel. Pixels corresponding to the same experiment were pooled together and resulting scatter-plots in the complex plane were linearly fitted using singular value decomposition. The fluorescence lifetime of the donor and the FRET efficiency was calculated as shifts in the scatter data representing photo-arrival time per pixel. The molar fraction of APT-mCitrine in complex with the substrate-mCherry was calculated using the scaled projection over the fitted line.
Additionally, samples expressing only mCitrine (τ = 3 ns) were measured in each experimental session to obtain the contribution of the instrument response function (IRF) to the first harmonic. By performing a reference measurement over several hours it was confirmed that the IRF properties were not changing significantly during the course of an experiment. To estimate avalanche photodiode dark-current, all samples were measured in the absence of laser excitation and resulting 'dark' photon-counts were used to calibrate the IRF. Moving structures of live cells during the ~150 second acquisition time for FLIM photon counting histograms were determined from fluorescence intensity images acquired at 2 seconds intervals on a separate photomultiplier tube (PMT) during the FLIM data acquisition. This sequence was compared to the integrated intensity image constructed from photons collected by APDs during the FLIM sequence and these low confidence regions with high variance (indicating movement) were masked in the ES/E_T image.

Metabolic Labelling, Click Chemistry and Western Blotting to detect Palmitoylation

MDCK cells were transfected with APT wt-6His or APTC2S-6His and incubated with 15-HDYA for 2h under standard culturing conditions. Protein lysates were prepared in RIPA Lysis buffer (Cell Signaling) with Protease inhibitors (Roche) and 100 mM PMSF. Lysates

were incubated on pre-equilibrated Ni-NTA beads (Qiagen) for 1h at 4°C and the beads were washed to remove aspecifically bound proteins. His-tagged APTs were then specifically eluted with 100 mM Imidazole and incubated at 37°C for 1h with 20 mM Cu(II) SO_4, 50 mM TCEP and 5 mM Biotin-azide for the Click reaction as described previously (6, 7). The reaction mixture was then incubated with SDS-Gel loading buffer (Pierce) for 15 minutes and processed via SDS-PAGE, blotted on a PVDF membrane, probed with Rabbit Anti-hAPT antibody followed by Donkey Anti-Rabbit IgG-IR Dye 680 and Streptavidin-IR Dye-800. The blot was scanned on a LiCOR Odyssey infra-red scanner and bands corresponding to APT/APTC2S were quantified for the Streptavidin/Anti-Rabbit IgG intensity ratio, indicating the level of palmitoylation.

Simulation of APT dynamics on the Golgi apparatus

In order to explore the effect of the negative feedback by the auto-depalmoylation of Golgi-localized APTs on the localization of palmitoylated substrates, we constructed a simple 2-compartment model consisting of 'Cytosol' and 'Golgi' compartments. The model incorporates the translocation of the substrate from the cytosol to the Golgi by palmitoylation through the action of palmitoyltransferases (PAT), and from the Golgi to the cytosol through depalmitoylation by acyl-protein thioesterase (APT). Similarly, APT may translocate between the cytosol and Golgi based on its palmitoylation status. The APT and PAT enzymatic activities were defined to have Michaelis-Menten kinetics.

$$[S_{Cyt}] \underset{\rightarrow}{^{V^S_{PAT}}} [S_{Golgi}] \quad \Rightarrow \quad V^S_{PAT} = \frac{\left((PAT)\cdot(k^{PAT}_{cat})\right)\cdot S_{Cyt}}{k^{PAT}_M + S_{Cyt}}$$

$$[APT_{Cyt}] \underset{\rightarrow}{^{V^{APT}_{PAT}}} [APT_{Golgi}] \quad \Rightarrow \quad V^{APT}_{PAT} = \frac{\left((PAT)\cdot(k^{PAT}_{cat})\right)\cdot APT_{Cyt}}{k^{PAT}_M + APT_{Cyt}}$$

$$[S_{Golgi}] \underset{\rightarrow}{^{V^S_{APT}}} [S_{Cyt}] \quad \Rightarrow \quad V^S_{APT} = \frac{\left(\left(\left(APT_{Golgi}\right)+\left(APT_{Cyt}\right)\right)\cdot(k^{APT}_{cat})\right)\cdot S_{Golgi}}{k^{APT}_M + S_{Golgi}}$$

$$[APT_{Golgi}] \underset{\rightarrow}{^{V^{PAT}_{APT}}} [S_{Cyt}] \quad \Rightarrow \quad V^{APT}_{PAT} = \frac{\left(\left(\left(APT_{Golgi}\right)+\left(APT_{Cyt}\right)\right)\cdot(k^{APT}_{cat})\right)\cdot APT_{Golgi}}{k^{APT}_M + APT_{Golgi}}$$

Where,

$\boldsymbol{S_{Cyt}}$, $\boldsymbol{S_{Golgi}}$, $\boldsymbol{APT_{Cyt}}$ and $\boldsymbol{APT_{Golgi}}$ are substrate and APT concentrations in the cytosol and Golgi, respectively.

V^S_{PAT} and V^S_{APT} are the reaction rates of the palmitoylation and depalmitoylation reactions for the substrate derived from literature(8, 37–39).

V^{APT}_{PAT} and V^{APT}_{APT} are the reaction rates of the palmitoylation and depalmitoylation reactions for APT.

PAT is the concentration of the palmitoyltransferase on the Golgi apparatus.

k_{cat}^{PAT} and k_M^{PAT} are the catalysis and Michaelis-Menten kinetic parameters of the palmitoyltransferase derived from literature (8-11).

k_{cat}^{APT} and k_M^{APT} are the catalysis and Michaelis-Menten kinetic parameters of the APT depalmitoylation activity.

Parameters in the model include:

- Relative volumes of the two compartments
- Concentrations of the substrate, APT and PAT species
- Michaelis-Menten kinetic constants of APT and PAT enzymatic activities (assumed to be the same irrespective of compartmental localization for simplicity)

Limitations exist with respect to availability and applicability of *in vitro* kinetic parameters and reliable measurements of volume and protein concentrations. Nonetheless, through reasoned approximation the parameter list was populated as follows:

Parameter	**Value**	**Units**
k_{cat}^{APT}	1-5	s^{-1}
k_{cat}^{PAT}	1	s^{-1}
k_M^{APT}	1	μM
k_M^{PAT}	1	μM
PAT	1-10	μM
APT	1-5	μM
Volume of Cytosol	1-10	pL
Volume of Golgi	0.01-0.1	pL

The Simbiology toolbox (MATLAB 2012a) was used to define a 2-compartment model consisting of a Cytosol and Golgi compartment, with translocation of species couple to enzyme activities. The concentrations of species were set to between 1-5 μM, while kinetic parameters for the APT thioesterase reaction as well as the palmitoyltransferase (PAT) reaction were derived from literature as mentioned earlier. Species concentrations were tested within this regime to ensure that simulation behavior does not change qualitatively. All species except the PAT are located in the Cytosol as the initial starting condition. The simulation is then allowed to reach steady state, where substantial concentrations are built up on the Golgi. Perturbations were applied as 'Doses' in the Simbiology toolbox. Perturbation

of up to an order of magnitude of APT and substrate concentrations in both compartments, and perturbations of the PAT activity in the Golgi compartment were tested. Sensitivity analysis was performed using ordinary differential equations over the course of simulation time.

The model is made available as a standard SBML file and a Simbiology project.

Bioinformatics

Human APT1 (Acc. ID: O75608) and APT2 (Acc.ID: O95372) sequences were retrieved from the UniProt database (12), and supplied to the CSS-PALM 3.0 (13) software for predictions of putative palmitoylation sites. Alignments for metazoan APT1 and APT2 were generated with the ClustalW algorithm using Jalview (14).

Supporting References

1. Currie, L.A. 1968. Limits for qualitative detection and quantitative determination. Application to radiochemistry. Anal Chem. 40: 586–593.

2. McNally, J.G. 2008. Quantitative FRAP in Analysis of Molecular Binding Dynamics In Vivo. In: Fluorescent Proteins. Academic Press. pp. 329–351.

3. Sprague, B.L., R.L. Pego, D.A. Stavreva, and J.G. McNally. 2004. Analysis of Binding Reactions by Fluorescence Recovery after Photobleaching. Biophys. J. 86: 3473–3495.

4. Smisdom, N., K. Braeckmans, H. Deschout, M. vandeVen, J.-M. Rigo, et al. 2011. Fluorescence recovery after photobleaching on the confocal laser-scanning microscope: generalized model without restriction on the size of the photobleached disk. J. Biomed. Opt. 16: 046021.

5. Tannert, A., S. Tannert, S. Burgold, and M. Schaefer. 2009. Convolution-based one and two component FRAP analysis: theory and application. Eur Biophys J. 38: 649–661.

6. Martin, B.R., C. Wang, A. Adibekian, S.E. Tully, and B.F. Cravatt. 2011. Global profiling of dynamic protein palmitoylation. Nat. Methods. 9: 84–89.

7. Rostovtsev, V.V., L.G. Green, V.V. Fokin, and K.B. Sharpless. 2002. A stepwise huisgen cycloaddition process: copper(I)-catalyzed regioselective “ligation” of azides and terminal alkynes. Angew. Chem. Int. Ed Engl. 41: 2596–2599.

8. Jennings, B.C., and M.E. Linder. 2012. DHHC Protein S-Acyltransferases Use Similar Ping-Pong Kinetic Mechanisms but Display Different Acyl-CoA Specificities. J. Biol. Chem. 287: 7236–7245.

9. Satou, M., Y. Nishi, J. Yoh, Y. Hattori, and H. Sugimoto. 2010. Identification and characterization of acyl-protein thioesterase 1/lysophospholipase I as a ghrelin deacylation/lysophospholipid hydrolyzing enzyme in fetal bovine serum and conditioned medium. Endocrinology. 151: 4765–4775.

10. Duncan, J.A., and A.G. Gilman. 1998. A Cytoplasmic Acyl-Protein Thioesterase That Removes Palmitate from G Protein α Subunits and p21RAS. J Biol Chem. 273: 15830–15837.

11. Yeh, D.C., J.A. Duncan, S. Yamashita, and T. Michel. 1999. Depalmitoylation of endothelial nitric-oxide synthase by acyl-protein thioesterase 1 is potentiated by Ca(2+)-calmodulin. J. Biol. Chem. 274: 33148–54.

12. The UniProt Consortium. 2009. The Universal Protein Resource (UniProt) 2009. Nucl Acids Res. 37: D169–174.

13. Ren, J., L. Wen, X. Gao, C. Jin, Y. Xue, et al. 2008. CSS-Palm 2.0: An Updated Software for Palmitoylation Sites Prediction. Protein Eng. Des. Sel. 21: 639–644.

14. Waterhouse, A.M., J.B. Procter, D.M.A. Martin, M. Clamp, and G.J. Barton. 2009. Jalview Version 2—a Multiple Sequence Alignment Editor and Analysis Workbench. Bioinformatics. 25: 1189–1191.